Journal of Sound and Vibration (2001) **248**(2), 289–314
doi:10.1006/jsvi.2001.3798, available online at http://www.idealibrary.com on IDEAL®

IDENTIFICATION OF HYSTERETIC SYSTEMS USING THE DIFFERENTIAL EVOLUTION ALGORITHM

A. KYPRIANOU AND K. WORDEN

Department of Mechanical Engineering, The University of Sheffield, Mappin Street, Sheffield S1-3JD, England. E-mail: k.worden@sheffield.ac.uk

AND

M. PANET

EDF DER MTC, 1 route de Sens, 77818 Moret/Loing, France

(*Received* 24 *September* 1999, *and in final form* 9 *March* 2001)

A widely used model in the field of hysteretic or memory-dependent vibrations is that of Bouc and Wen. Different parameter values extend its use to various areas of mechanical vibrations. As a consequence an identification method is required to identify the parameter values relevant to its application. Its structure, however, includes internal states and non-linear terms. This rules out the conventional identification methods, such as least squares and maximum likelihood because they require derivative calculations of the prediction error with respect to the parameters. In this paper are presented some results for Bouc–Wen model identification, using simulated noise-free data, simulated noisy data and experimental data obtained from a nuclear power plant. The method used to achieve this is the differential evolution algorithm. Differential evolution (DE) is an optimization method developed to perform direct search in a continuous parameter space without requiring any derivative estimation.

1. INTRODUCTION

Hysteretic or memory-dependent phenomena are observed in many areas such as magnetism, electricity, material, phase transitions and elasto-plasticity of solids [1]. In mechanical vibrations, the elasto-plasticity of some vibrating components introduces non-linearities which can be identified as of hysteretic type. A model, which describes accurately many random non-linear vibrations of the above type, is the Bouc–Wen model. In the context of the forced single-degree-of-freedom oscillator of equation (1) z is the hysteretic restoring force.

$$m\ddot{x} + c\dot{x} + kx + z = f(t), \tag{1}$$

where m, c and k are the mass, damping and spring coefficients respectively. The hysteretic restoring force z is given by the Bouc–Wen model of

$$\dot{z} = -\alpha|\dot{x}|z^n - \beta|z^n|\dot{x} + A\dot{x}, \quad n \text{ odd},$$

$$\dot{z} = -\alpha|\dot{x}|z^{n-1}|z| - \beta\dot{x}z^n + A\dot{x}, \quad n \text{ even}. \tag{2}$$

0022-460X/01/470289 + 26 $35.00/0

The model was firstly introduced by Bouc in its rudimentary form with n equal to unity [2]. This was able to describe the hysteresis loop peculiar to the relationship between the restoring force, z, and displacement, x. The parameters α and β govern the shape of the loop. Wen generalized the Bouc equation to its final form by introducing the parameter n as given in equation (2) [3]. This parameter controls the smoothness of the hysteresis loop. The parameter A contributes to the linear stiffness of the oscillator.

Owing to the versatility of this model to represent various shapes of hysteresis loops, it has attracted much attention in the area of hysteretic vibrations. As a consequence the model is studied for various parameter sets in order to fit in different applications. Therefore, a need emerges to identify the parameters for each different case.

In this article, first, a literature survey of the aspects related to the identification of systems with hysteresis is presented followed by a presentation of the most commonly available parameter estimation methods with their rationale. This leads to the indication that certain classes of these methods are unable to be used in identification tasks similar to the one presented in this paper.

Afterwards, a relatively new method, based on DE is presented and proposed for the parameter estimation of the Bouc–Wen model. Finally, this paper concludes with the presentation of identification results using the DE on simulated noise-free data, on simulated noisy data and on experimental data. A discussion of these results is given along with their presentation.

2. LITERATURE SURVEY

2.1. GENERAL DESCRIPTION OF THE BOUC–WEN MODEL AND PARAMETERS EFFECT

The Bouc–Wen model is capable of producing different hysteretic behaviours and is also amenable to random vibration analysis. These tests dictate the two major paths research over the years has followed: one of them is that of the parameter identification and the other one is the analytical determination of the response of the Bouc–Wen model to random excitations for various parameter sets. This is related to aspects of random process theory.

As has been already mentioned, Bouc [2] introduced the model of equation (2) for $n = 1$ in order to model random hysteretic vibrations. Ten years later, Wen [3] generalized this to the form in equation (2). In the same paper, Wen went on and presented some typical hysteretic loops that the model produces, for the case of $n = 1$. In addition, he showed some initial loading paths of the model and that for $n = \infty$ when it represents an ideal elastic–plastic system. Then, relying on the fact that an input of independent arriving pulses (shot noise) to a system causes the system to respond with a Markov random process, he used the Fokker–Planck [4] equation to estimate the probability that a particular response vector will occur. Consequently, he used the Galerkin procedure to obtain the solution of the Fokker–Planck equation for both the stationary and non-stationary cases. He concluded his article by showing some comparative results obtained from a Monte Carlo simulation.

Briefly, equivalent linearization is the procedure of obtaining a linear system that will provide a response close to that of the studied non-linear system. The inadequacy of the Krylov–Brogoliubov method of equivalent linearization of wideband models, led Wen [5] to propose a new method of doing this. The technique he used, substitutes the third order non-linear system of equations (1) and (2) with a linear third order system whose parameters are obtained from the minimization of the mean-square error. This method can easily be extended to multi-degree-of-freedom systems. As he did with his previous paper he went on

and applied this method to the model with certain parameter values and then compared the results with Monte Carlo simulation. In addition, in this paper he finalized the proposal made in his previous paper [3] by re-modifying the Bouc–Wen model to take into account the post-yield stiffness. He actually introduced the parameter v as shown in equation (3), to represent the ratio of prior to post-yield stiffness. Equation (3) represents a single-degree-of-freedom system with m, c and k representing the corresponding mass, damping and stiffness and z the hysteretic force.

$$m\ddot{x} + c\dot{x} + vkx + (1 - v)z = f. \tag{3}$$

Pivovarov and Vinogradov [6] in their paper expressed the Bouc model, i.e., $n = 1$, in stress and strain terms in order to describe the constitutive relation of a dry friction damper, namely the Stockbridge damper. Without analyzing in detail the effect of the parameters on the hysteretic loops they used equivalent linearization techniques to obtain the backbone curves. The backbone curves chart the deviation of the non-linear resonance frequencies from the linear one as the amplitude excitation increases. Then, using these curves they identified parameter values to represent their experimental data. They concluded that the parameter α is associated with the resonance of the overall system and β with the non-linearities. They did not mention the effect of the sum of these two parameters and how their relative values affect the dynamics.

2.2. IDENTIFICATION

2.2.1. *Non-parametric*

Non-parametric system identification means that an experimental response of a system, to an input, can be identified with a particular model response to the same input. For example, the presence of non-linearity will introduce behaviours such as subharmonics, superharmonics, resonance frequency shifts and chaos. If a particular model is known to produce such effects then it can be used to give an identity to certain experimental data that entail the same behaviour. Therefore, the essence is not on the parameters of the equations of motion but on the actual response of the system.

Lo *et al.* [7] used a method relying on deconvolution to estimate the non-linear hysteretic force z from experimental records. Afterwards they used a method similar to the restoring surface method, reference [18], to plot a corresponding surface of the estimated force z. They stressed the importance of the selection of the appropriate independent variables over which the surface will be drawn. This is because hysteretic systems are multi-valued response systems and the common restoring force method fails for such systems. They suggested to draw the surface of $\dot{z}$ versus $\dot{x}$ and z. It is obvious that the nature of the surface is determined by the non-linear function of $\mathrm{d}z/\mathrm{d}x$. A polynomial fit to this surface at the end will reveal the parameters associated with the given experimental records. Afterwards they quoted how the parameter combinations of α and β for $n = 1$ govern the hardening or softening of the particular system. Finally, they applied this method to identify the parameters and simulate better a friction-type isolator.

This surface method implies that if an estimation of the non-linear force z is achieved by deconvolution, then it should be possible to identify the parameter n from the polynomial shape the surface $\mathrm{d}z/\mathrm{d}x$ is supposed to have.

Wong *et al.* [9] studied the multi-harmonic steady state oscillation of the Bouc–Wen model. They used the Galerkin–Levenberg–Marguard method to obtain frequency response functions from swept sine waves. They found that superharmonic frequencies

occur always in the Bouc–Wen model's response to periodic forcing. Then they went on to quote that in the cases of subharmonic resonances, a chaotic behaviour is associated. Finally, they reported that during non-zero mean periodic input, the response is non-zero mean as well.

In their companion paper [10] they performed a similar dynamic analysis over five different hysteresis loops obtained by appropriate parameter values. They studied how the superharmonics are affected by the parameters' values. Afterwards they showed how the Bouc–Wen model is used as a constitutive equation for components with plasticity in a similar way as in reference [6]. Finally, they inspected for role of v (equation (3)) in the constitutive equation of stress and strain and they found that for $v > 0$ the hysteresis loop depends on stress and strain as well.

2.2.2. *Parametric*

Parametric identification puts the importance on the parameters of the equation of motion and aims to identify their values from experimental records. In order to ensure success in the identification of the values of the parameter of a certain model, its parameters should be identifiable in the sense that two different parameter vectors give two different responses.

Andronikou *et al.* [11] discussed the concept of identifiability of hysteretic systems. The main line of their approach was to prove that there are equivalent linear and non-linear systems that are identifiable in the sense of the first paragraph for systems with bilinear hysteresis. After they proved the existence of those models they went on to demonstrate the conditions of the identifiability for the equivalent systems. They finalized their paper by presenting and proving a theorem, which says that once the equivalent linear and non-linear systems are identifiable then the original hysteretic bilinear system is identifiable as well. This result is a sufficient condition for a hysteretic bilinear system to be identifiable but not necessary, since the opposite is not proved, i.e., if a hysteretic bilinear system is identifiable there exists a linear or non-linear equivalent model that is identifiable as well.

The fact that the Bouc–Wen model can be equivalently linearized might be able to provide the sufficient condition required for identifiability. In addition, the circumstance, under which the Bouc–Wen model represent bilinear hysteresis, strengthens even more the case that its parameters are identifiable.

Sues *et al.* [12] obtained the hysteretic force z numerically and then used it to formulate an error sequence. They carried on and obtained estimated parameters using the least-squares method. The availability of z renders the error equation differentiable and the solution of normal equation direct.

Yar and Hammond [13] used the Gauss–Newton iterative method to solve the normal equations derived from their formulation of the least-squares problem. They, then relying on their error formulation, gave a theorem about the asymptotic properties of the sampling of the estimates. Also, from this point of view they discussed the identifiability of the parameters. Afterwards, they presented simulated results together with the variance and covariance of the estimates. They also quoted the importance of input level to certain parameters.

Masri *et al.* [14] presented an adaptive method to identify Bouc–Wen's model once experimental data are available on-line. This has been achieved by using neural networks through a specially designed adaptive law. In the same paper, they presented simulated and experimental results together with model validation.

Andronikou *et al.* [15] as a successor to the paper [11] about the identifiability of hysteretic systems used a random method to search directly the parameter space in order to

identify their proposed models of bilinear hysteresis. They also stress that the success of identifying the parameters is very much dependent on the input level.

In the same tenor, Deacon and Worden [16] apply genetic algorithms to search the parameter space of the Bouc–Wen model. They showed simulated results for the case of constant n. In addition, they presented a picture of fitness landscape for the parameters α and β.

3. PARAMETER ESTIMATION METHODS

Generally, the aim of every model is to predict the relevant experimental observed data. In this case, it is assumed that the Bouc–Wen model (2) in connection with the model of one-degree-of-freedom oscillator (1) predicts the experimentally observed hysteretic acceleration time histories $\ddot{x}(t)$. Different parameter sets $\underline{P}$ produce various models which in turn give different predictions of time histories $\hat{\ddot{x}}(t|\underline{P})$.

In order to assess the goodness of the prediction the difference between the predicted output $\hat{\ddot{x}}(t|\underline{P})$ and the reference experimental $\ddot{x}(t)$ output is used. Hence, a prediction error or cost can be defined [17, 18] as

$$\varepsilon(t) = \ddot{x}(t) - \hat{\ddot{x}}(t|\underline{P}). \tag{4}$$

The prediction error ε defined in equation (4) can serve as a means of comparison between different models. A selection of model for which the sequence of the prediction errors becomes as small as possible is the aim of parameter identification methods.

Over the years, several methods have been developed to select the best possible model. The ones extensively used are mentioned here with their rationale. The least-squares method finds the smallest possible sequence of error by trying to minimize a scalar measure [19]

$$OF = \frac{1}{n}\sum_{i=1}^{n} (\ddot{x}(i) - \hat{\ddot{x}}(i|\underline{P}))^2, \tag{5}$$

where n is the number of data points.

By taking the derivatives of equation (5) with respect to the parameters and equating them to zero one arrives at a set of n equations with n_p unknowns (n_p is the number of parameters). Their solution gives the required parameter values. Suppose that prediction error (4) has a conditional probability density function depending on time t, parameter set $\underline{P}$, and the input. In addition, assume that there are no equation disturbances. This assumption renders the prediction errors independent for two different time instants [17]. Assuming that the probability density function (PDF) for an individual instant is given by an arbitrary function g, the joint probability density function for all the error values is given by

$$JPDF = \prod_{i=1}^{n} g(\ddot{x}(i) - \hat{\ddot{x}}(i|\underline{P})). \tag{6}$$

The value of this function gives the probability that the output $\hat{\ddot{x}}(t|\underline{P})$ of the model at t is the output of the system. If one refers to the parameter vector $\underline{P}$, equation (6) is known as the likelihood of the parameter vector to give a model that replicates the system output. This function therefore, needs to be a maximum in order to give a suitable estimate of the parameter vector. Hence, the parameter vector which maximizes equation (6) is called the maximum likelihood estimate.

Finally, the prediction error sequence $\varepsilon(t)$ can be made small when a parameter estimate $\underline{P}$ gives a sequence that is not correlated with another sequence $\zeta(t)$ containing information relevant to the identified system. Generally, this is formulated as

$$\frac{1}{N}\sum_{i=1}^{N}\varepsilon(t|\underline{P})\zeta^{\mathrm{T}}(t)=0. \tag{7}$$

The solution of equation (6) with respect to $\underline{P}$ gives the required parameter estimate $\underline{\hat{P}}$. Intuitively, this means that the predictors $\hat{\bar{x}}(t|\bar{P})$ utilize all the information at time t, rendering the prediction error independent of the system information contained in $\zeta(t)$. The sequence $\zeta(t)$ contains the *instruments* to obtain $\underline{\hat{P}}$ and the method is known as the instrumental variable method.

The above methods work well when the system is linear in the parameters and therefore analytic in them. This is because they require the calculation of the derivatives of the objective function with respect to the parameters. In such cases, the complexity only increases with the number of parameters to be identified, as the linearity ensures quadratic objective functions. The continuity ensures the existence of the derivatives.

For *non-linear in the parameters* systems the resulting error equations, as discussed above, are non-linear. This means that the objective functions are not quadratic, possessing a single global minimum; the necessary and sufficient conditions for the existence of minimum can be satisfied for various parameter sets [20]. This results in local minima which in turn might attract the solution into one of them depending on the starting position. Non-linearity also makes it necessary to use iterative schemes, which collect local gradient information or a Hessian matrix. In cases, however, of discontinuous types of non-linearity or/and unobservable states, estimation of the gradients or the Hessian matrix is not feasible.

In such cases a different approach should be sought that does not require any derivative calculations. These methods can be classified as heuristic or direct search since they rely on the objective function evaluations only. In the literature there are many such methods available such as in the Nelder and Mead downhill simplex [21], genetic algorithms and simulated annealing [20]. The nature of the Bouc–Wen model, however, dictates a more robust and at the same time reliable and fast algorithm. The Nelder and Mead method performs well locally but is trapped in local minima easily. When simulated annealing is incorporated in the Nelder and Mead method on similar optimization tasks as those in this paper, it does not improve much [22]. Genetic algorithms are designed to work on a discrete parameter space [23, 24]. In this case, any attempt to discretize parameters can only increase the complexity of the problem. Hence, for this study an optimization algorithm was sought which is capable of utilizing concepts borrowed from genetic algorithms and the Nelder and Mead method and exploits their strengths. This is found in the differential evolution algorithm [22, 25], which uses the concept of the Nelder and Mead method of acquiring information from within a vector population combined with evolutionary methods similar to those of genetic algorithms [23, 24]. A more detailed description of differential evolution follows.

4. DIFFERENTIAL EVOLUTION

DE is basically very similar to conventional genetic algorithms (GAs). The differences are in the way the mechanisms of mutation and crossover are performed using real floating point numbers instead of long strings of zeros and ones. The following is a brief description of the DE method.

In comparison with GAs the basic difference lies in the scheme for generating trial parameter vectors [22, 25]. The importance of the *term-trial parameter vector* will be evident in the following paragraphs. Figure 1 shows schematically the basic operations of the DE working on optimization of a hypothetical single-degree-of-freedom system. The parameter vectors are composed of the three well-known parameters: mass (M), damping (C) and spring (K).

The algorithm starts with an initial pool of 15 three-dimensional vectors drawn from uniform probability distributions. The uniform probability density ensures that the

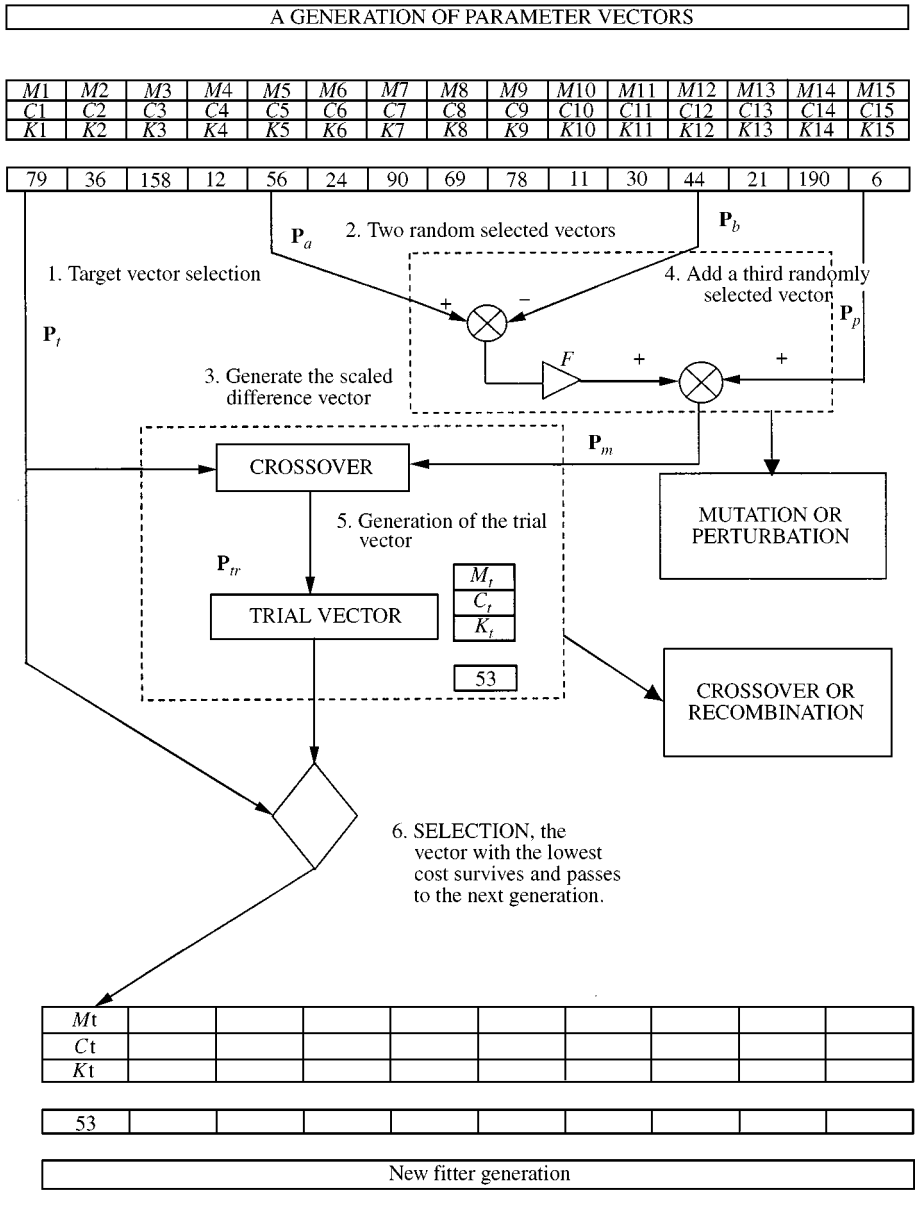

Figure 1. An iteration of differential evolution.

parameter vectors generated will span the space equally. The initial pool acts as the initial *generation* from which the whole operation of evolution starts.

DE mutates (perturbs) a randomly selected member $\mathbf{P}_p$ of the featured generation with *vector differentials* as demonstrated for the two-dimensional case in Figure 2. Each differential is the difference, between two randomly selected vectors ($\mathbf{P}_a$ and $\mathbf{P}_b$), scaled with a parameter F. $\mathbf{P}_a$ and $\mathbf{P}_b$ should not be either the target vector $\mathbf{P}_t$ or the selected for mutation vector $\mathbf{P}_p$. This process generates a new mutated vector $\mathbf{P}_m$ (Figure 1).

The survival value of each gene (parameter) is numerically formed by the action of recombination as indicated in Figure 3. DE implements this by using a series of number of parameters (NP) binomial experiments on two vectors. These are the parents and the new generated vector, the child. The two parents are (1) the target vector $\mathbf{P}_t$ and (2) the mutated vector $\mathbf{P}_m$. Each binomial experimental event determines the parent the child takes its genes (parameters) from. The likelihood that governs the inheritance of the *trial* parameter vector $\mathbf{P}_{tr}$ is determined by a constant parameter designated as the *crossover ratio* (CR). In this case, there are two mutually exclusive events. Event A: a specified parameter is taken from one parent with odds (CR: 1) or event B: the same parameter is taken from the other parent with odds ((1 − CR): 1) (Figure 3). It is obvious that the child cannot take a particular parameter from both of the parents. The generating child is called the *trial vector* $\mathbf{P}_{tr}$.

Natural selection in differential evolution is implemented via a comparison process between the cost of the trial vector and the cost of the target vector. The fittest one, in this case the one with lowest objective value, passes to the next generation. Performing this sequence of operations on every single member of each generation, differential evolution

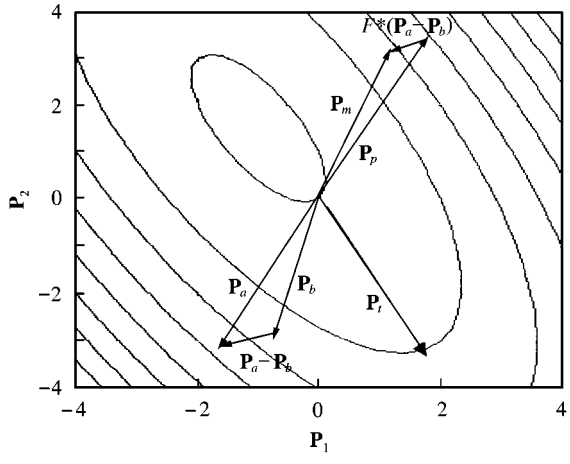

Figure 2. 2-d perturbation process of the differential evolution.

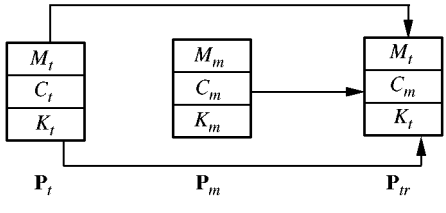

Figure 3. The crossover operation.

generates a new set of 15 three-dimensional vectors. This set is simply a new generation with improved characteristics.

Iterating the above procedure results in new fitter generations. The iteration halts when a stopping criterion is satisfied. Usually, this is set as either a desired objective value or a maximum number of iterations or both.

5. THE OBJECTIVE FUNCTION

5.1. THE MEAN SQUARE ERROR (MSE)

The objective function used for this study is the mean square error. The mean square error, for a general predicted time history $\hat{x}(t)$ compared to the respective measured (reference) time history $x(t)$, can be cast in the discrete normalized form as

$$MSE = \frac{100}{n\sigma_{\tilde{x}}^2} \sum_{i=n}^{n} (x(t) - \hat{x}(t|\underline{P}))^2, \tag{8}$$

where $\sigma_{\tilde{x}}^2$ is the variance of the measured output and n the number of points in the measured output.

5.2. OPTIMIZATION

Following the discussion above, what remains to complete the task of identifying the best parameter set for a model structure to predict the measured data correctly is the optimization of the criterion function. In this case, the optimization problem can be stated as, from reference [20].

Obtain the parameter vector $\hat{\underline{P}}$ which minimizes the MSE. The parameter vector is subjected to the constraint

$$\underline{P}_{min} \leqslant \hat{\underline{P}} \leqslant \underline{P}_{max}. \tag{9}$$

5.3. PENALTY FUNCTION

The so-called direct search optimization methods do not usually provide a mechanism to restrict the parameters in the range defined by inequality (9); neither does the differential evolution. However, an unconstrained optimization method can be transformed to a constrained one using the concept of the penalty function. This function determines a penalty to be added to the value of the MSE any time any parameter exceeds the range limits. The penalty function selected for this case is given by equation (10). Figure 4 shows the effect of the penalty function in trying to constrain the parameter in the region of 10–30. Notice the rapid increase of the penalty as the parameter diverges from the bounds of the range and the difference of the rate of change at either end. At the lower end this is higher because the coefficient of the square difference is higher.

$$\text{Penalty } (P_i) = \begin{cases} 20((P_{i(min)} - P_i)/P_{(min)})^2 & \text{for } P_i < P_{i(min)}, \\ 0 & \text{for } P_{i(min)} \leqslant P_i \leqslant P_{i(max)}, \\ 20((P_{i(max)} - P_i)^2/P_{i(max)})^2 & \text{for } P_i > P_{i(max)}. \end{cases} \tag{10}$$

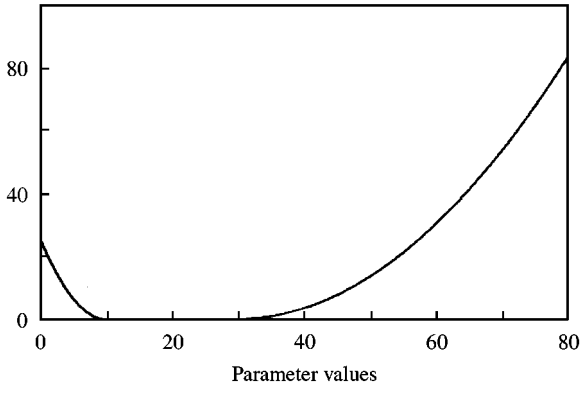

Figure 4. The penalty function.

6. IDENTIFICATION OF BOUC–WEN MODEL WITH SIMULATED NOISE-FREE DATA

6.1. PROBLEM FORMULATION

The single-degree-of-freedom system of equations (1) and (2) can be cast in the state space form as follows. First, define the state variables: displacement as z_1, i.e., $z_1 = x$, velocity z_2, i.e., $z_2 = \dot{x}$ and the hysteretic force z. A single-degree-of-freedom system with hysteresis is now presented by equation (11). Note that the parameter n was kept constant to the value of 2, as it has been found through experimentation that this value enables the model to capture better the dynamics of the data used in this paper.

$$\dot{z}_1 = z_2, \qquad \dot{z}_2 = (f - cz_2 - z)/m, \qquad \dot{z} = -\alpha|z_2|z|z| - \beta z_2 z^2 + Az_2. \tag{11}$$

In this case, the output is considered to be the displacement z_1 and the reference output z_1^{ref} the response of equation (11) for the parameter vector $\underline{P}_{ref} = [1\ 20\ 1{\cdot}5\ -1{\cdot}5\ 6680]^{\mathrm{T}}$. The input force $f(t)$ is a Gaussian random input of root mean square value of $9{\cdot}92N$. The hysteretic force is non-observable and hence it has to be estimated. That is, the system becomes non-linear in the parameter vector $\underline{P}$ because some of its components are multiplied with z which is not known as well. In addition, all the simulations are assumed to start with zero initial conditions, as otherwise the initial conditions need to be estimated. In this respect the mean square error (8) is expressed as

$$MSE(\underline{P}) = \frac{100}{N\sigma^2_{z_1^{ref}}} \sum_{i=1}^{N} (z_1^{ref} - \hat{z}_1(\underline{P}))_i^2. \tag{12}$$

6.2. COMPUTATIONAL DETAILS

Differential evolution is programmed as an m-file in Matlab® whereas the model is developed in Simulink®. Adam's method is used as the numerical integrator [25]. The time histories were sampled at 250 Hz giving a time step of $\Delta t = 0{\cdot}004$ s.

The searching range for each parameter was extended to an order of magnitude above and below the reference value. For example the searching range for c was from 2 to 200 since its reference value is 20. In the case in which the optimization method estimates values out of the specified range, the penalty value of equation (10) is added to the MSE.

Each generation consisted of 30 members ($\underline{P}$) and each run was allowed to evolve to the 200th generation.

6.3. RESULTS

6.3.1. *Results with range of one order of magnitude*

Table 1 shows the optimization results with the parameter range being extended one order of magnitude to either end of the true parameter vector $\underline{P}$. In Table 1, $\underline{P}_i$ is the optimized parameter vector and $\underline{P}_{ref}$ the reference one. The vector with the optimized vector with the lowest MSE is given in the column with heading $\underline{\mathbf{P}}_{LMSE}$. The mean optimized vector of over 100 runs is given in the column with $\underline{\hat{\mathbf{P}}}_{MEAN}$ as heading whereas the standard deviation of the standard deviation vector of the optimized set is given in the column $\underline{\hat{\mathbf{P}}}_{STD}$.

The lowest MSE for these results is 0·0208%. A comparison between the hysteresis loops and predicted displacements for the parameter vector with the lowest MSE and the reference parameter vector is shown in the plots of Figure 5. Seeking more accurate results the range of the parameters has been reduced. Based on Table 1 the mean and standard deviation of the parameters define a new smaller range according to

$$\underline{\hat{\mathbf{P}}}_{MEAN} - \underline{\hat{\mathbf{P}}}_{STD} \leqslant \underline{\hat{\mathbf{P}}}_i \leqslant \hat{\mathbf{P}}_{MEAN} \geqslant \underline{\hat{\mathbf{P}}}_{STD}. \tag{13}$$

6.3.2. *Results of the first reduced range*

The lowest MSE in this case is 0·0025%. A comparison between the hysteresis loops and predicted displacements for the parameter vector with the lowest MSE and the reference parameter vector is shown in the plots of Figure 6.

Applying equation (13) to the results of Table 2, a new smaller range can be defined. This leads to more accurate results as depicted in the next section.

6.3.3. *Results of the second reduced range*

The results of the second reduced range are shown in Table 3.

The lowest MSE is 1·332e − 10%. Note that the hysteresis loop and time histories are not shown for this case because the optimized parameters have insignificant difference from the reference ones. Therefore, the optimized and the reference plots are the same.

TABLE 1

Optimization results for the range of one order of magnitude

$\underline{\mathbf{P}}_i$	$\underline{\mathbf{P}}_{ref}$	$\underline{\hat{\mathbf{P}}}_{LMSE}$	$\underline{\hat{\mathbf{P}}}_{MEAN}$	$\underline{\hat{\mathbf{P}}}_{STD}$
M	1	0·9915	1·0652	0·1313
C	20	20·2800	20·6660	2·0141
α	1·5	1·4210	1·8135	0·6843
β	− 1·5	− 1·4330	− 4·0760	3·5959
A	6680	6636	6964	847·20

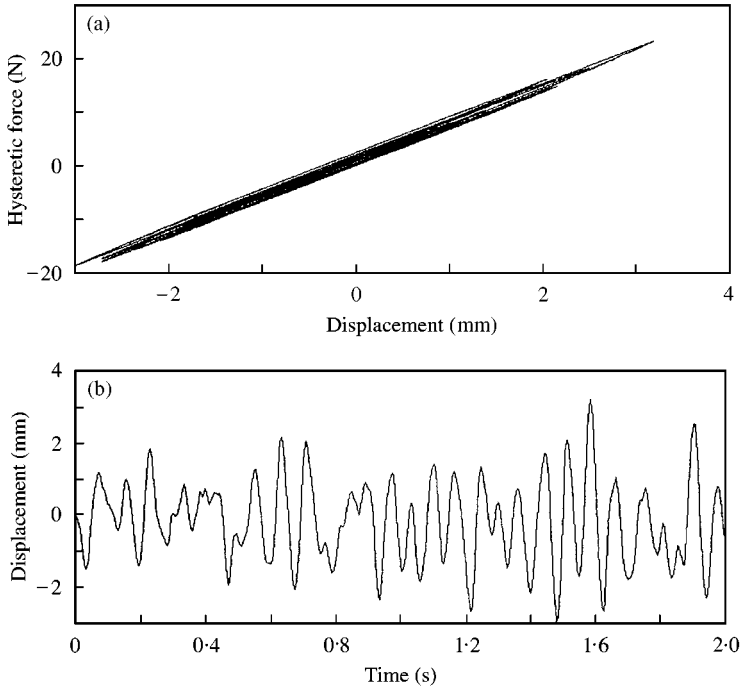

Figure 5. Comparison of the optimized results with the reference ones for: (a) hysteretic force; (b) displacement, key: ——, reference signal; – – –, optimized signal.

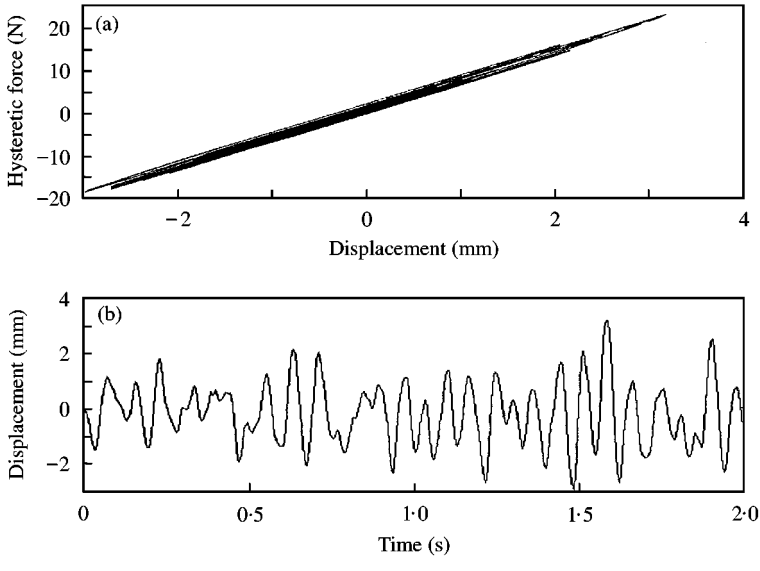

Figure 6. Comparison of the optimized results with the reference ones: (a) Hysteretic force; (b) displacement, key: ——, reference signal; – – –, optimized signal.

TABLE 2

Optimization results of the first reduced range

$\underline{\mathbf{P}}_i$	$\underline{\mathbf{P}}_{ref}$	$\hat{\underline{\mathbf{P}}}_{LMSE}$	$\hat{\underline{\mathbf{P}}}_{MEAN}$	$\hat{\underline{\mathbf{P}}}_{STD}$
M	1	1·0010	1·0009	0·0030
C	20	19·9500	19·9656	0·0475
α	1·5	1·4850	1·4863	0·0148
β	− 1·5	− 1·3660	− 1·4863	0·1337
A	6680	6690	6685	20·151

TABLE 3

Optimization results of the second reduced range

$\underline{\mathbf{P}}_i$	$\underline{\mathbf{P}}_{ref}$	$\hat{\underline{\mathbf{P}}}_{LMSE}$	$\hat{\underline{\mathbf{P}}}_{MEAN}$	$\hat{\underline{\mathbf{P}}}_{STD}$
M	1	1·0000	1·0003	0·0016
C	20	20·0000	19·9824	0·0310
α	1·5	1·5000	1·4937	0·0094
β	− 1·5	− 1·5000	− 1·4965	0·0856
A	6680	6680	6681	8·0826

7. NOISE STUDY

7.1. STUDY OUTLINE

A similar procedure, as for the identification of the hysteresis model 11 with noise-free simulated data, was followed for the identification of the same model with simulated data that have been corrupted by noise. For the case of output noise $v(t)$ the reference time history z^{ref} was obtained by direct addition of $\underline{v}$(t) on the reference displacement z_1^{ref} of section 6.1, i.e., the response of model (11) with parameter values $\underline{P}_{ref} = [1\ 20\ 1{\cdot}5\ -1{\cdot}5\ 6680]^{\mathrm{T}}$ to the excitation force. Equation (14) shows how z_1^{ref} is corrupted by $v(t)$, where v represents the component of $v(t)$ at each particular time.

$$z^{ref} = z_1^{ref} + v. \tag{14}$$

In this circumstance the mean-square error becomes

$$MSE(\underline{P}) = \frac{100}{N\sigma^2_{z_1^{ref}}} \sum_{i=1}^{N} (z^{ref} - \hat{z}_1(\underline{P}))_i^2. \tag{15}$$

The optimization was performed for different levels of noise $v(t)$. As a measure of the noise level the percentage noise-to-signal ratio NSR, as in equation (16) was used, namely,

$$NSR(v(t)) = (\sigma(v(t))/\sigma(z_1^{ref}))100. \tag{16}$$

The noise-to-signal ratio *NSR* for the output error case $v(t)$ was determined based on the level of the standard deviation of the displacement response $\sigma(z_1^{ref})$ of model (11) for the parameter values $\underline{P}_{ref} = [1\ 20\ 1{\cdot}5\ -1{\cdot}5\ 6680]^{\mathrm{T}}$.

A zero mean Gaussian of unity standard deviation (0, 1), sequence was generated in Matlab® and then was scaled according to the *NSR*. Equation (17) shows how the scaling multiplier was obtained. Note that the multiplier is just the desired noise standard deviation.

$$\sigma(v(t)) = NSR(v(t))\sigma(z_1^{ref})/100. \tag{17}$$

The identification was performed for the following levels of *NSR*: 0·1, 1, 10, 20, 40, 60, 80 and 100%. Those levels were chosen arbitrarily but in such a way as to scan the entire spectrum of the noise vividness. The results obtained are shown in section 7.2 and they are discussed in section 7.3.

7.2. RESULTS

Table 4 shows the identified parameters of the models with noise applied to the output, equation (14), at the levels mentioned in the previous section. The table shows the results of the lowest mean square error of 20 runs. Figure 7 consists of two columns of four boxes each. Each box contains an overlay plot of the noisy reference z^{ref} with the corresponding optimized time history. The noise-to-signal ratio *NSR*, is indicated at the bottom of each box.

7.3. DISCUSSION OF THE RESULTS

From Table 4 it can be concluded that the mean-square error, *MSE*, of the optimized parameters remains lower than 1% when *NSR* is below 10%. In the case in which the noise-to-signal ratio exceeds 10%, the *MSE* increases drastically and proportionally with *NSR* level. At *NSR* 100% the *MSE* is 49·57%.

The situation discussed above is mirrored in the plots of Figure 7. It can be seen that the optimized response for *NSR* levels of 20% and above is badly matched with the noisy reference. The situation becomes even more severe at higher levels of *NSR*, as indicated in the last three plots of the left column.

TABLE 4

Identified results with the noise applied to the output

Reference noise level (%)	$m = 1$	$c = 20$	$\alpha = 1{\cdot}5$	$\beta = -1{\cdot}5$	$A = 6680$	$MSE(\hat{\underline{P}})(\%)$
0·1	1·00	19·99	1·50	− 1·47	6685	$1{\cdot}54 \times 10^{-4}$
1	0·99	19·96	1·50	− 1·61	6682	*0·01*
10	0·99	19·90	1·50	− 1·12	6701	*0·98*
20	0·9993	20·19	1·54	− 1·41	6679	*3·88*
40	0·98	20·00	1·47	− 2·07	6583	*13·63*
60	0·99	19·43	1·54	− 0·95	6765	*26·03*
80	1·01	20·01	1·52	− 2·03	6790	*39·89*
100	0·98	20·07	1·52	− 0·66	6631	*49·57*

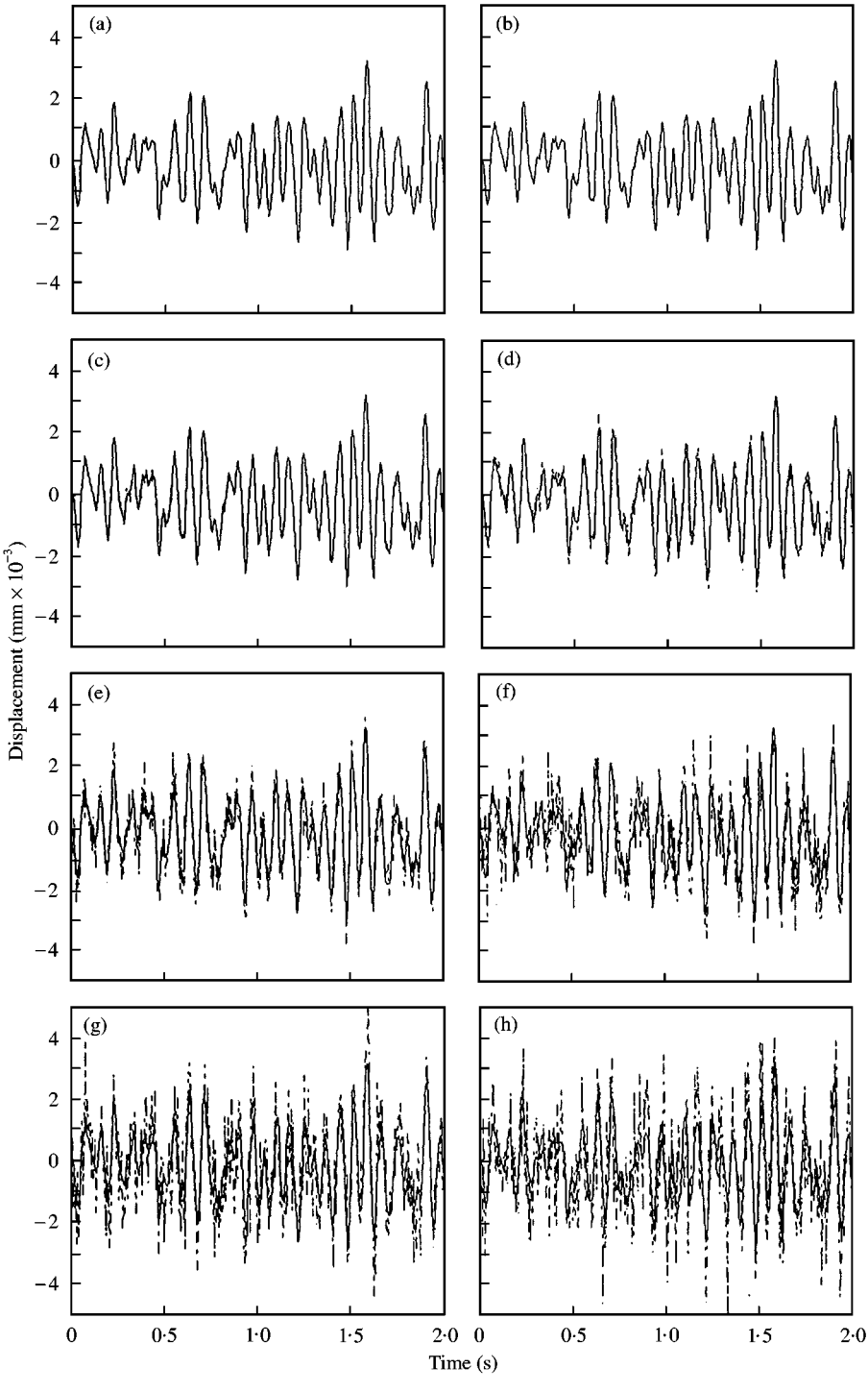

Figure 7. Overlay plots of the reference time history with the optimized one. NSR values (%): (a) 0·1; (b) 1·0; (c) 10·0; (d) 20·0; (e) 40·0; (f) 60·0; (g) 80·0; (h) 100·0. (a) Hysteretic force and (b) displacement, key: ——, reference signal; – – –, optimized signal.

The main objective of every identification method is to identify a model that gives an output that explains all the characteristics due to the input. When the output is corrupted by additive noise that is not correlated to any extent with the model equations, it is obvious that the model is not able to predict its existence simply because it is not possible to get anything out of nothing.

On this account the optimization is based on those characteristics of the reference output that would have shown if the noise was absent. Hence, the optimized parameter vectors will be closer to the ones optimized in the noise-free case, i.e., the true ones as shown in Table 4. In this way, however, at high noise levels the response of the model will be mismatched with the reference one, yielding high optimized mean-square errors. In such a case, the effective remedy is to improve the measurement process or filter the noise.

Finally, it can be summarized that for additive output noise the identification method gives good parameter estimations at the expense of good model predictions. For the noise added in the model equations the identification method gives a model capable of accurate predictions at the expense of good parameter estimation.

8. IDENTIFICATION WITH EXPERIMENTAL RESULTS

8.1. EXPERIMENTAL DATA

The French electricity authority (Electricité de France, EDF) obtained the experimental data used for identification, from an earthquake resistance test of a nuclear power plant. The plant underwent low-frequency seismic excitation provided by a SOPMEA input floor. Figure 8(a) shows a demonstration of such a test. The important part of the plant is the response of the valve (RCV292VP MASONEILAN) identified by point 5 in Figure 8(b).

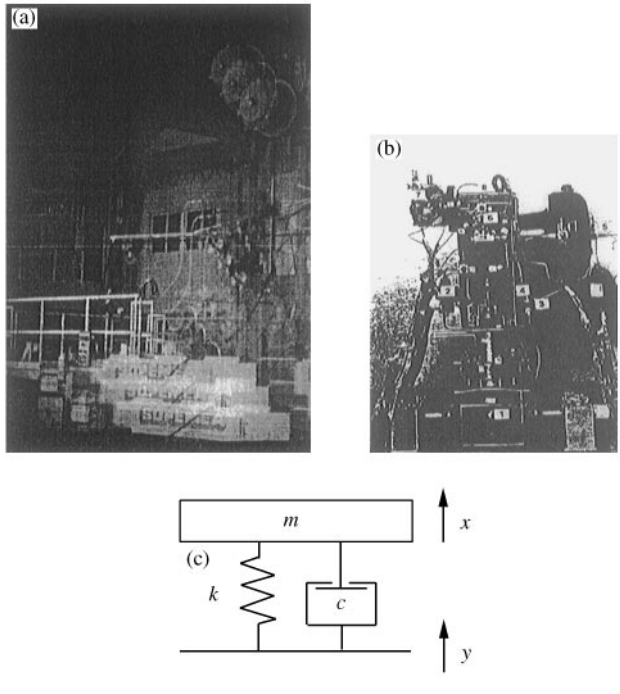

Figure 8. Experimental set-up: (a) nuclear plant vibration; (b) value response (point 5); (c) oscillator model.

In this context, the experimental data consist of the absolute seismic acceleration input $\ddot{y}$ and the relative response acceleration u of the valve to the base; i.e., it can be modelled as an oscillator with a movable base (Figure 8(c)). Figure 9 depicts the experimental transmissibility curves for two different inputs at two amplitude levels as shown in Figure 10. It is obvious that for a single-degree-of-freedom system to behave in this way, it should possess some kind of non-linearity. The curve with the lowest peak corresponds to the high-level input, showing that the non-linearity accounts for an increase of the damping as the level of the input increases. A slight downward shift to the resonance frequency is also perceptible, a fact which indicates softening.

8.2. THE BEST LINEAR SYSTEMS

The equation of motion of the system in Figure 8(c) is given by equation (18) and is

$$\ddot{u} + P_1\dot{u} + P_2 u = -P_3\ddot{y}, \tag{18}$$

where $P_1 = 2\zeta\omega_n$ (damping s^{-1}); $P_2 = \omega_n^2$ (square of the natural angular frequency $(\text{rad}/s)^2$; $P_3 = \mu$ (a participation factor).

Assuming that the experimental transmissibility curves shown in Figure 11 are produced from two different systems, it is possible to identify the best linear system (Figure 8(c)) representing the above characteristics. This will yield additional information about the system in terms of the parameter differences. For example, a system optimized with the low-level signal will have particular damping, P_1, and natural frequency P_2 values. Any changes to these values after the optimization with the higher level input signal will give indications about the nature of the non-linearity involved. The optimization results of Table 5 were obtained.

In over 30 runs the parameter estimates did not change values before the first decimal point. This is because the linearity of the model structure forces a single global minimum.

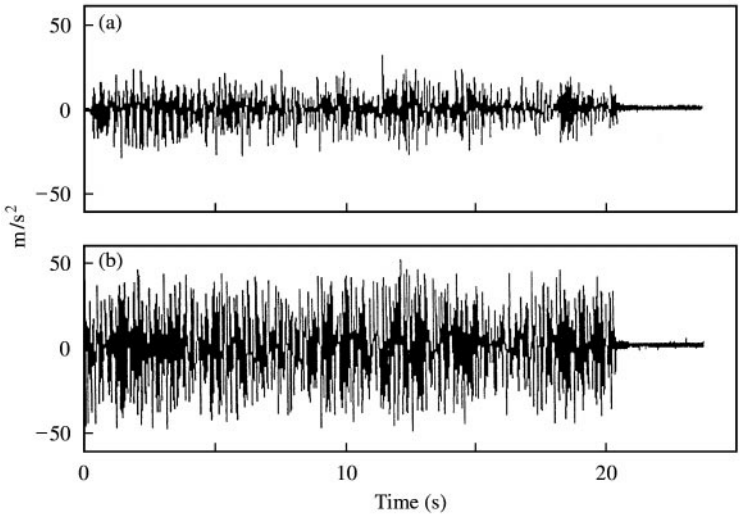

Figure 9. The time histories of the experimental inputs.

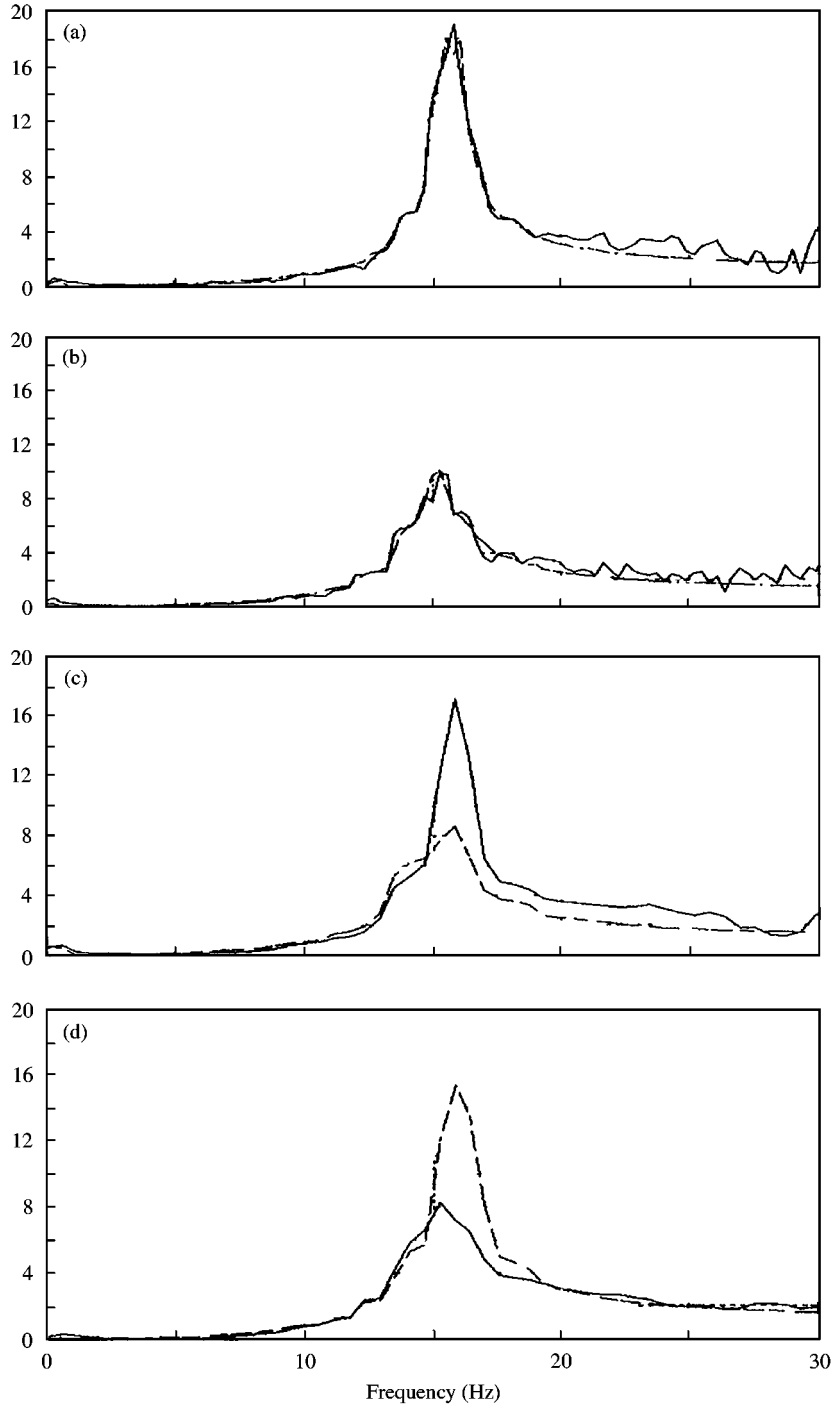

Figure 10. Frequency-domain results of linear system for experimental signal (——) and optimized signal (– – –): (a) low-level optimization; (b) low-level experimental, high-level optimization; (c) high-level experimental, low-level optimization; (d) high-level experimental.

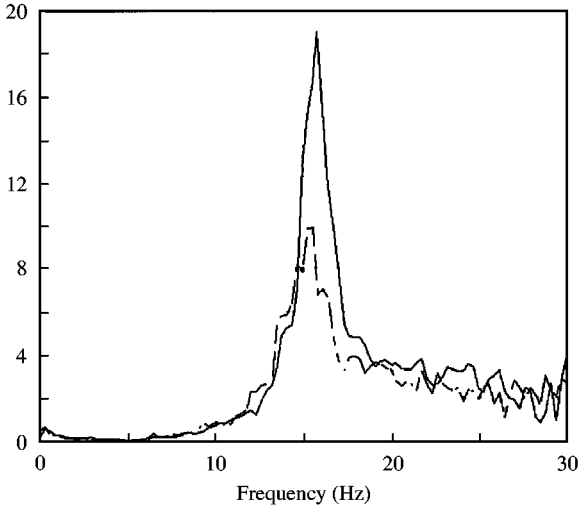

Figure 11. Experimental transmissibility curves for low seismic input (dsd) (——) and high seismic input (sdd) (– – –).

TABLE 5

Optimized results for the best linear system (*italic letters indicate the cross mean-square errors*)

	$\mathbf{P}_1$	$\mathbf{P}_2$	$\mathbf{P}_3$	Mean-square error (%)
Low amplitude	5·42	9687	1·22	12.87
	(*11·87*)	(*9021*)	(*1·51*)	(*45·07*)
High amplitude	11·87	9021	1·15	16·10
	(*5·42*)	(*9687*)	(*1·22*)	(*41·87*)

It is obvious that there are linear systems representing the dynamics adequately for both the cases. Although two different linear models are used in order to represent data recorded from the same experimental component, some useful conclusions can be drawn.

First, the frequency domain results were excellent for each of the inputs separately as portrayed by the accurate match of the first two plots of Figure 10. On the other hand, the last two plots of Figure 10 show that the model optimized for one input cannot represent the dynamics of the other. This means that the linear models capture the values of natural frequency and damping ratio correctly, as expected, for each input separately but they fail to capture their change as the amplitude varies.

Second, the time domain predictions for the low-amplitude optimization almost overlay the measured data in the two time intervals shown in the first two plots in Figure 12. For the high-amplitude optimization there are some deviations in the interval 9–10 s shown in the first two plots of Figure 13. This explains why the lower amplitude optimization gave a mean-square error lower than the higher amplitude one. The last two plots of Figures 12 and 13 verify the observation pointed out previously; the dynamics of the system change as the amplitude of the input varies.

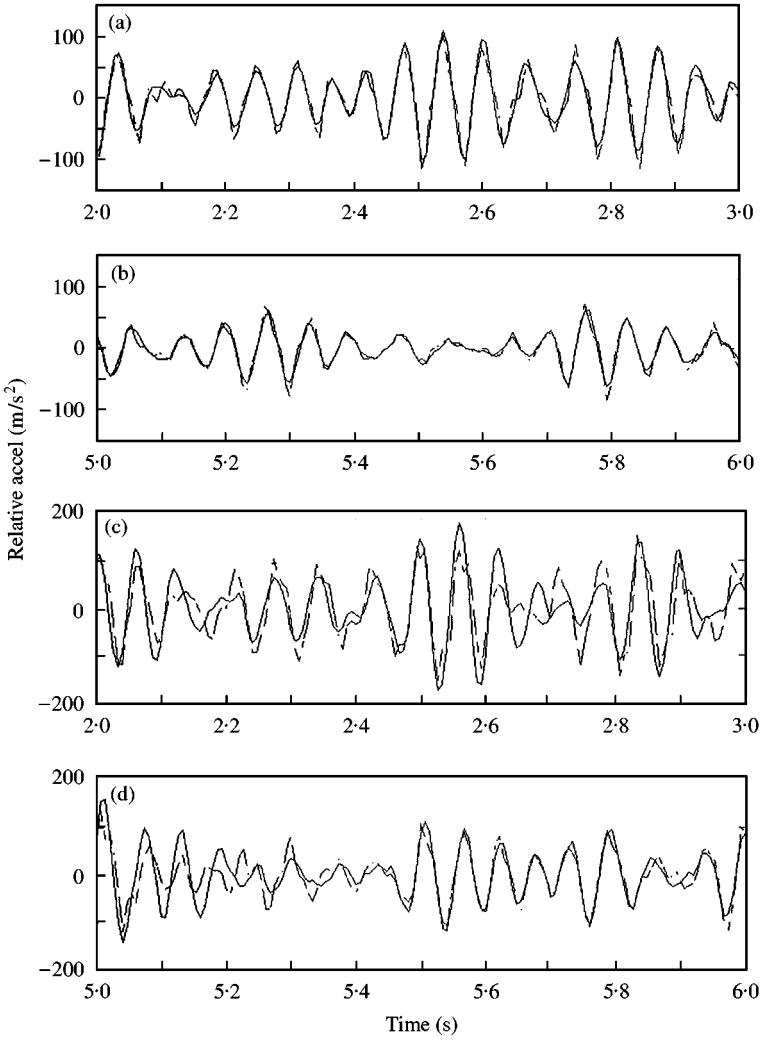

Figure 12. Time-domain results for the optimized low-level linear model. The upper plots are the response of the low-level input. The lower plots show the response of the low-level model to the high-level input. Key for traces: ——, optimized; – – –, experimental.

The lack of a very good fit at lower amplitudes for the high-input case (Figure 13) is an indicator of non-linearity in the system. In other words at low amplitudes the dynamics are different from those at high amplitudes. Therefore, the parameter estimates are different for the two cases. Furthermore, from Figure 13 it is obvious that the non-linearity is excited when the response is above 100 m/s^2. To elucidate this, it can be noted that between 9·08 and 9·12 s of the second plot of Figure 13 the system is governed by the linear dynamics which possess the lower damping ratio 5·14%. However, because of the higher amplitudes involved, the damping estimated is higher. Therefore, the peaks at lower levels of the optimized signal will be lower than those should be expected or, otherwise, achieved by 5·14% damping ratio.

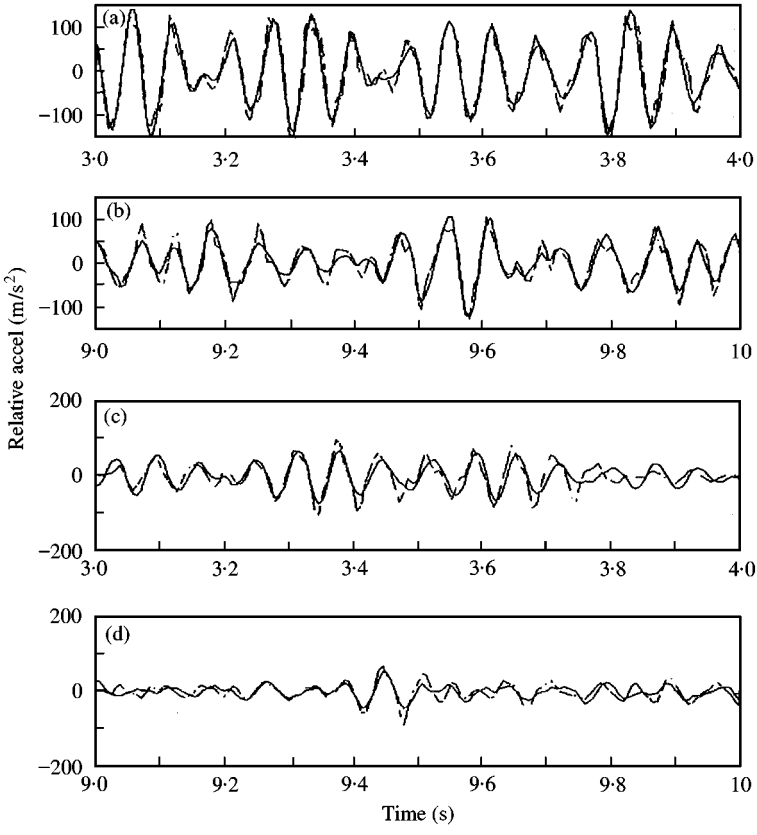

Figure 13. Time-domain results for the optimized high-level linear model. The first two plots are the response of the high-level input. The last two plots show the response of the low-level input. Key for traces: ——, optimized; – – –, experimental.

8.3. THE BOUC–WEN MODEL FOR THE EXPERIMENTAL DATA

To compensate for all the effects that result from the analysis of the previous section the Bouc–Wen hysteretic model was used. The equations of motion are now altered as follows:

$$\ddot{u} + g(\dot{u}, u) = -P_3\ddot{y}, \quad g(\dot{u}, u) = P_1\dot{u} + P_2 u + z(u), \tag{19, 20}$$

$$\dot{z}(u) = P_4\dot{u} - (P_5|\dot{u}||z|z + P_6\dot{u}|z|^2), \tag{21}$$

where $P_1 = 2\zeta\omega_n$, $P_2 = \omega_n^2$, $P_3 = \mu$, $P_4 = A$, $P_5 = \alpha$ and $P_6 = \beta$. The damping ratio, the natural angular frequency and the participation factor of the oscillator are denoted by ξ, ω_n and μ respectively. The parameters A, α and β are those associated with the Bouc–Wen model.

8.3.1. *Identification with the low-level input*

Using the low-level input the following parameter values gave the lowest mean-square error: $P_1 = 4{\cdot}767$, $P_2 = 9457$, $P_3 = 1{\cdot}275$, $P_4 = 487$, $P_5 = 4{\cdot}2 \times 10^6$ and $P_6 = 9 \times 10^6$ giving a mean-square error (MSE) of 11·17%. The response of the system with these values of the high input level gives an MSE of 41.10%. Comparing these values for the linear case (Table 5)

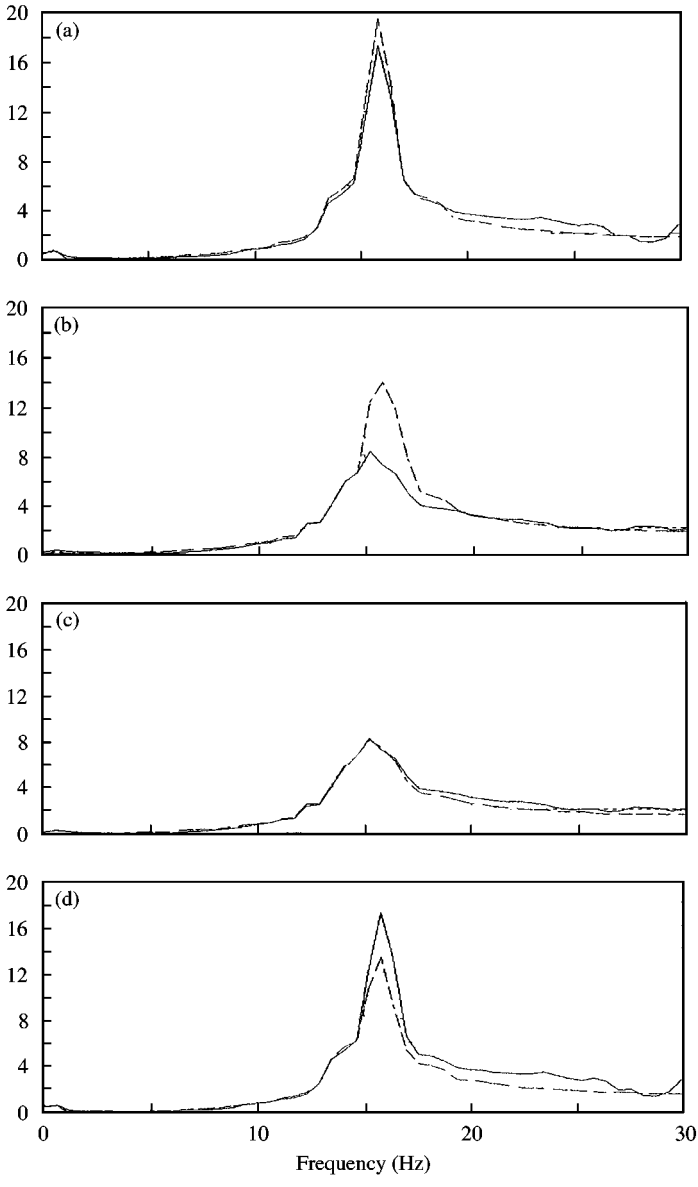

Figure 14. Frequency domain results (——, experimental; – – –, optimized) of the two-step identification method. The first two plots show the results of the first step (identification using the low-level amplitude input). The last two plots show the results of the two-step identification method.

which gave MSE 12·87% for the low-level amplitude input and 45·07% for the high-level amplitude a marginal improvement is observed. The first two plots of Figure 14 show the frequency domain results for this case. It is obvious that the curves match for the low-level case but do not for the high-level input. Time domain results in Figure 15 indicate the same effect. Therefore, the low-level input signal alone is not sufficient for experimental identification.

In an attempt to overcome the above problem the following procedure was devised: optimize all the six parameters of equations 20–22 by using the low-level amplitude input

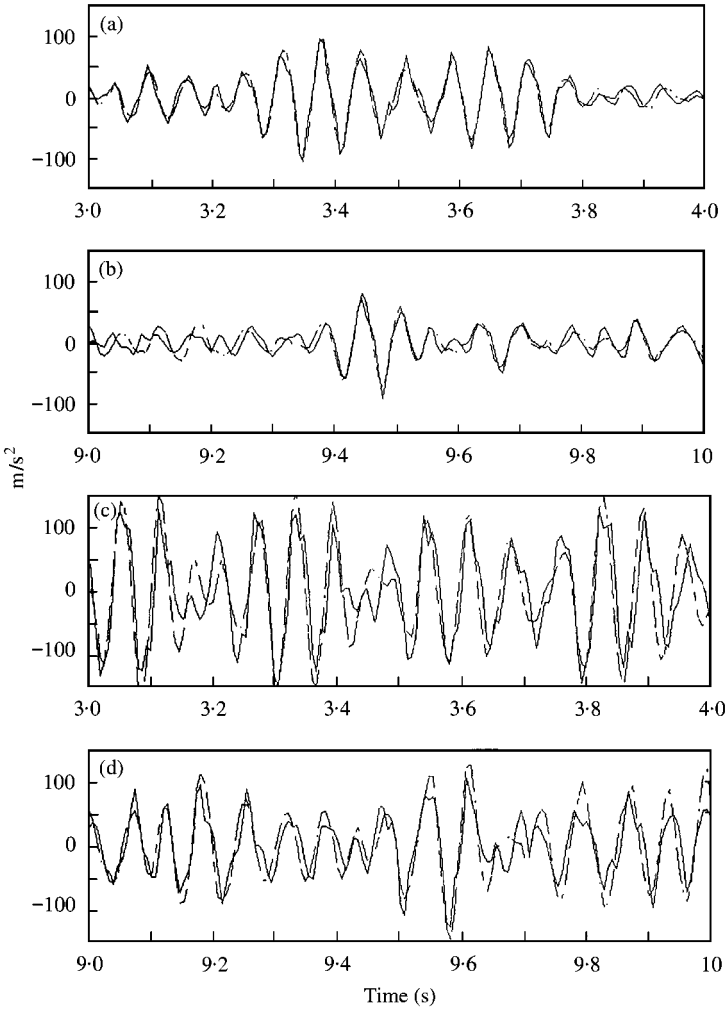

Figure 15. Time-domain results of the first step of the two-step identification method. First two plots: response to low-level input. Last two plots: response to high-level input. (——, experimental; – – –, optimized).

signal (first step). This will optimize the linear part of the model and possibly some effects of the non-linearity. Then start the optimization with the high-level input using as initial population the one optimized by the low-level input, exciting in this way the non-linearity. This will cause the non-linear parameters to be optimized and the linear ones (those optimized first) to be fine tuned. In this way, it is expected to obtain parameter estimations for both high- and low-amplitude regimes. This leads to a two-step identification method.

8.3.2. *Identification using the high-level input*

Following the tenor of the previous paragraph, the last generation of the previous optimization is passed as the startup generation for this input.

The results obtained are $P_1 = 5{\cdot}83$, $P_2 = 5677$, $P_3 = 1{\cdot}12$, $P_4 = 487$, $P_5 = 110 \times 10^6$ and $P_6 = 174 \times 10^6$. The associated mean-square errors for these parameter values are 11·12% for the high-level input case and 20% for the low level. There is a significant improvement in

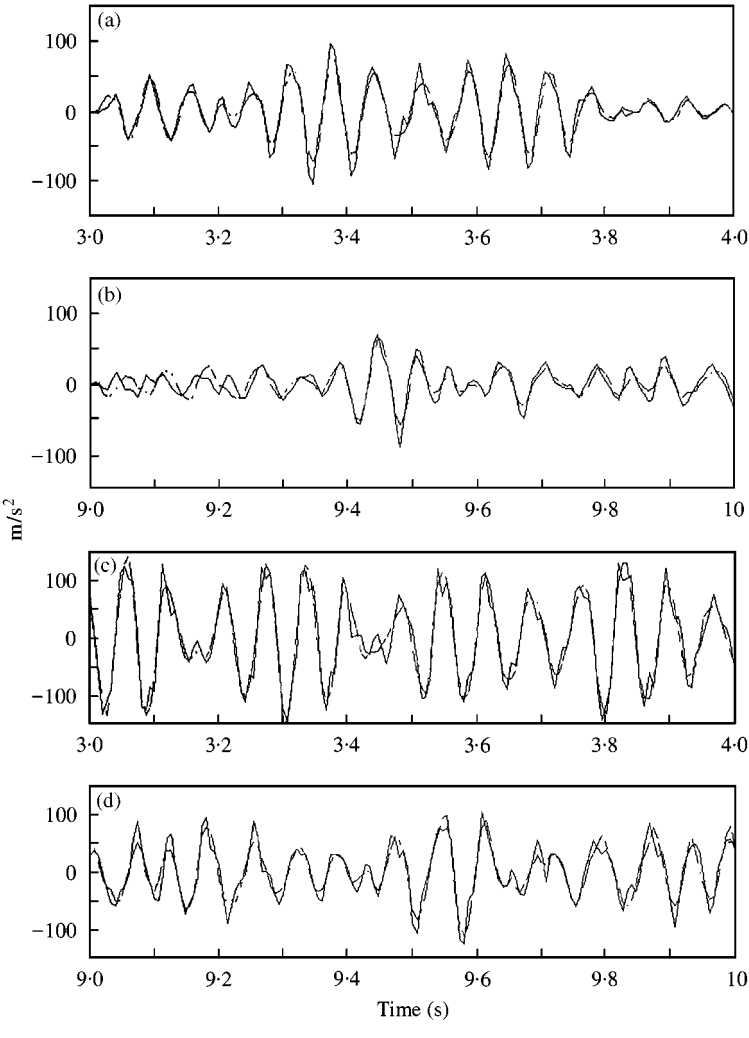

Figure 16. Time domain results of the second step of the two-step identification method. First two plots: response to low-level input. Last two plots: response to high-level input. (——, experimental; – – –, optimized).

the mean-square error values compared with the corresponding ones from Table 5. For the high amplitude level the error drops from 16·1 to 11·1% whereas for the low-level amplitude case the error drops from 41·87 to 20%. The last two plots of Figures 14 and 16 show the relevant frequency and time domain results, respectively, whereas Figure 17 depicts the hysteresis loops caused by the two different inputs.

Optimization of the low-level input signal alone gives a good fit for itself but not for the high-level input as shown in Figure 15. This is because the low-level input signal does not excite persistently the non-linear hysteretic state. After the failure of the first step to capture the span of dynamic effects involved, the two-step procedure was suggested.

Thinking in terms of the parameter space it can be argued that the parameters of the system after the first step are in the proper neighbourhood of the space. The linear parameters are optimized but the non-linear ones are not. By using the high input level the directions of the parameters shrink to a valleys in the parameter space. The optimization algorithm then pushes the parameters towards the desired minimum.

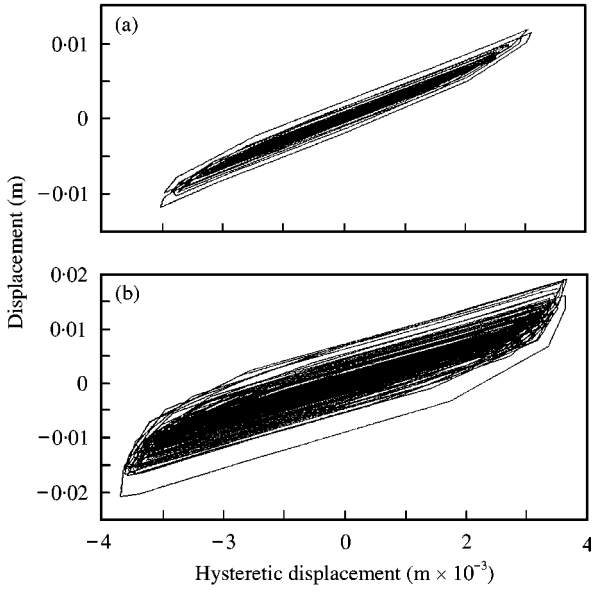

Figure 17. Hysteretic displacement loops obtained from the optimized model.

It can be argued that the two-step procedure is more reliable. The effect of increasing the damping is captured as the amplitude increases as well as the frequency shift. This is because the hysteresis, shown in Figure 17, is stronger for higher inputs.

9. CONCLUSIONS

Identification of the Bouc–Wen parameters using simulated data gave excellent results. The differential evolution identified successfully the global minimum defined by the reference parameter vector. The perfect match of the time histories of the reference and identified parameter vectors validates the statement that the differential evolution identified the global minimum.

For both the experimental data sets, excellent linear models can be identified which capture the frequencies and damping at the individual amplitudes. However, linear models cannot capture the change of the dynamics as the amplitude changes. The Bouc–Wen model was used to capture this effect. The failure of the low amplitude level input to identify parameters that give accurate prediction for the high amplitude level input also forced the definition of the two-step procedure. This procedure reduced significantly the cross mean-square errors, giving acceptable responses for both amplitude levels as shown in Figure 17. The relatively high mean-square errors can be ascribed to the fact that the response of the model at some time instants mismatches the experimental response mainly because of the noise. In addition, there might exist dynamics that left unmodelled something that the high values of the parameters P_5 and P_6 suggest. Finally, Figure 17 indicates that the hysteretic effect is substantial.

REFERENCES

1. A. VISITIN 1994 *Differential Models of Hysteresis*. Berlin: Springer.
2. R. BOUC 1967 *Proceedings of the Fourth Conference on Non-Linear Oscillations, Prague*, 315. Forced vibrations of mechanical systems with hysteresis.

3. Y. K. WEN 1976 *Journal of the Engineering Mechanics Division* **102**, 249–263. Method of radom vibration of hysteretic systems.
4. A. PAPOULIS 1991 *Probability Random Variables and Stochastic Processes*. Singapore: Mc-Graw-Hill.
5. Y. K. WEN 1976 *Journal of the Applied Mechanics Transactions of American Society of Mechanical Engineers* **47**, 150–154. Equivalent linearization for hysteretic systems under random excitation.
6. I. PIVOVAROV and G. O. VINOGRADOV 1987 *Journal of Sound and Vibration* **118**, 209–216. One application of Bouc's model for non-linear hysteresis.
7. H. R. LO, J. K. HAMMOND and M. G. SAINSBURY 1988 *Proceedings of the 6th International Modal Analysis Conference, FL*, Vol. II, 1453–1459. Non-linear system identification and modelling with application to an isolator with hysteresis.
8. S. F. MASRI and T. K. CAUGHEY 1979 *Journal of Applied Mechanics* **46**, 455–447. A non-parametric identification technique for non-linear dynamic problems.
9. C. W. WONG, Y. Q. NI and J. M. KO 1994 *Journal of Engineering Mechanics* **120**, 2271–2298. Steady state oscillation of hysteretic differential model. I: Response analysis.
10. C. W. WONG, Y. Q. NI and J. M. KO 1994 *Journal of Engineering Mechanics* **120**, 2299–2325. Steady state oscillation of hysteretic differential model. II: Performance analysis.
11. A. M. ANDRONIKOU, G. A. BEKEY and F. Y. HADAEGH 1983 *Journal of Dynamic Systems, Measurement, and Control* **105**, 209–214. Identifiability of non-linear systems with hysteretic elements.
12. R. H. SUES, S. T. MAU and Y. K. WEN 1988 *Journal of Engineering Mechanics* **114**, 833–846. System identification of degrading hysteretic restoring forces.
13. M. YAR and J. K. HAMMOND 1987 *Journal of Sound and Vibration* **117**, 161–172. Parameter estimation for hysteretic systems.
14. S. F. MASRI, A. SMYTH and A. G. CHASSIAKOS 1995 *Proceedings of the International Symposium on Microsystems, Intelligent Materials and Robots, Japan*, 419–422. Adaptive identification for the control of systems incorporating hysteretic elements.
15. A. M. ANDRONIKOU, G. A. BEKEY and S. F. MASRI 1982 *IFAC identification and System Parameter Estimation, Washington D.C.*, 331–336. Identification of non-linear hysteretic systems using random search.
16. B. DEACON and K. WORDEN 1996 *EUROMECH—second European Nonlinear Oscillation Conference, Prague*. Identification of hysteretic systems using genetic algorithms.
17. L. LJUNG 1982 *IFAC Identification and System Parameter Estimation, Washington D.C.*, 57–64. Identification methods.
18. P. YONG 1981 *Automatica* **17**, 23–39. Parameter estimation for continuous time models—a survey.
19. V. STREJC 1980 *Automatica* **16**, 535–550. Least squares parameter estimation.
20. S. S. RAO 1996 *Engineering Optimization: Theory and Practice*. New York: Wiley Interscience.
21. J. A. NELDER and R. MEAD 1965 *Computer Journal* **7**, 308–313. A simplex method for function minimisation.
22. R. STORN and K. PRICE 1997 *Journal of Global Optimization* **11**, 341–359. Differential evolution—a simple and efficient heuristic for global optimization over continuous spaces.
23. M. MITCHEL 1996 *An Introduction to Genetic Algorithms*. Cambridge, Massachusetts: The MIT Press, Massachusetts Institute of Technology.
24. K. WORDEN and B. P. DEACON 1996 *Identification in Engineering Systems, Proceedings of the Conference held at Swansea*, 499–509. Genetic parameter estimation.
25. K. PRICE and R. STORN 1997 *Dr. Dobb's Journal* **264**, 18–24. Differential evolution.
26. W. H. PRESS, S. A. TEUKOLSKY, W. T. VETTERLING and B. P. FLANNERY 1995 *Numerical Recipes in C the Art of Scientific Computing*. Cambridge: Cambridge University Press.